Proceedings of the 28th IEEE
EMBS Annual International Conference
New York City, USA, Aug 30-Sept 3, 2006

Flattening the Abdominal Aortic Tree for Effective Visualization

Joong Ho Won[1], Geoffrey D. Rubin[2] and Sandy Napel[1,2]
Departments of [1]Electrical Engineering and [2]Radiology, Stanford University, CA 94305, USA
{jhwon,grubin,snapel}@stanford.edu

Abstract— **We developed a novel visualization method for providing an uncluttered view of the abdominal aorta and its branches. The method abstracts the complex geometry of vessels using a convex primitive, and uses a sweep line algorithm to find a suboptimal placement of the primitive. The method was evaluated using 10 CT angiography datasets and resulted in a clear visualization with all cluttering intersections removed. The method can be used to convey clinical findings, including lumen patency and lesion locations, in a single two-dimensional image.**

I. INTRODUCTION

We developed and evaluated a method to visualize the abdominal aorta and its branches, as might be captured by Computed Tomography and Magnetic Resonance Angiography (CTA, MRA), in a single two-dimensional (2D) image. In the diagnoses of vascular abnormalities, it is often desirable to inspect all clinically relevant branches at the same time. However, conventional methods, such as Maximum Intensity Projection (MIP) and Volume Rendering (VR), require projection of the three-dimensional (3D) structure onto a 2D display plane, often causes misleading false intersections of vessels. Typical methods for resolving these "vessel crossings" are to try several projection directions in turn, or to examine only small portions at a time, either of which requires user interaction.

Visualization of the lumen of a single vessel is most often accomplished using Curved Planar Reformatting (CPR). The main idea of CPR is to "flatten" the ruled surface [1] defined by the centerlines of the vessel and a chosen scanning direction onto the display plane. However its extension to multiple vessels is challenging because the ruled surfaces of individual vessels virtually never coincide with each other. Kanitsar *et al.* proposed two remedies to this problem: one involved compositing each individual CPR with additional depth information (multipath CPR) while allowing significant overlap, while the other relaxed the spatial configuration in order to achieve non-overlapping branches (untangled CPR). The latter method hierarchically encloses the centerlines of vessels by circular sectors ("vessel hulls") and rotates them until the overlap between two sectors disappears. The resulting collection of vessel hulls is used to resample the voxels of the volume data in order to provide CPR-like images.

In this paper we propose an untangled visualization that builds upon the second approach by Kanitsar *et al.* To make better use of limited display, we cast the problem as one of prioritizing resources, where one decides beforehand which vessel segments should suffer relatively little distortion, and these are placed in priority order. In addition, while Kanitsar's method worked well in the peripheral vasculature, it sometimes results in non-convex vessel hulls when applied to aortic branches within the abdomen and pelvis, violating one of its internal assumptions and resulting in exhaustion of display. Our method overcomes this by finding suboptimal placements of individual hulls and not utilizing the hierarchical enclosure approach.

The following section explains the proposed method in detail. We present an evaluation of the method over several test cases in section III. Discussion of the results and the concluding remarks follow thereafter.

II. METHODS

A. Model Building

We represent the canonical anatomy of the abdominal aortic tree as a binary tree. For each node of the data structure, we associate a centerline of the corresponding vessel segment. We assume that each centerline is stored as an ordered set of n sample points $\{P_1, P_2, \cdots, P_n\}$ on a smooth 3D curve, where the sample size n varies from vessel to vessel. The order follows the direction of blood flow, so that P_1 corresponds to the proximal branching point (from the parent segment) and P_n corresponds to the distal branching point (toward the child segment) or the dangling endpoint. The proposed method assumes such a geometry-associated binary tree as an input to the algorithm. Given the relatively simple topology of the canonical anatomy, the required data structure can be built either manually or automatically by using a simple graph matching method.

B. Vessel Hull Primitive

The vessel hull geometric primitive is adopted from [2]. A vessel hull is the minimum-angle circular sector that encloses a projected vessel centerline $\{p_1, p_2, \cdots, p_n\}$, where p_i are a projection of the point P_i on the corresponding 3D centerline. The sector has its origin at the first sample point p_1 and the radius being $\|p_n - p_1\|$. The vessel hull requires that the distance from the center p_1 to p_i increases along with the index i. We met this requirement by employing the mapping used in the stretched CPR [3], which has an additional advantage with respect to untangling. Since the mapping is one-to-one, this "stretching" is free of self-intersection in a single vessel which may occur in the orthographic projection.

This work was supported by the National Institutes of Health under grant proposals 1R01HL67194 and 1U54GM072970.

1-4244-0033-3/06/$20.00 ©2006 IEEE.

It is also guaranteed that the center angle of the vessel hull is less than 180 degrees, meaning that the hull is always convex. One can think of a vessel hull as a conservative but convenient alternative to the convex hull of a projected centerline.

Given an input binary tree, the "stretching" is applied to each of the associated 3D centerlines and the vessel hull primitives are constructed. The output of this step is a binary tree with the same topology as the input but with 2D geometry abstracted by the vessel hulls. Notice that this step involves a slight relaxation of spatial configuration since the projected centerlines are forced to maintain the branching structure, *i.e.*, the proximal point of a child vessel must coincide with the distal point of the parent. The "stretching" is performed along the principal direction of each individual vessel to minimize the loss of spatial coherency. The resulting 2D tree may still exhibit intersections of the projected centerlines, and it is the task of the next step to remove them by minimally relaxing the spatial configuration of the vessel hulls.

C. Untangling

1) Prioritization of Placement: We view the untangling problem as a resource allocation one. As the 2D viewing plane is inherently restricted compared to the 3D space, overlapping vessels can be treated as contending for the same resource. A typical solution to such a resource conflict is to assign priorities to the subjects of conflict and allocate the resource according to those priorities. In our problem, a priority assignment can incorporate clinical significance and/or convention. For example, the aorta, iliac, and renal arteries occur in relatively predicable positions when viewed from a given, say, anterior-posterior, direction, with other branches, *e.g.*, the celiac, splenic, and mesenteric arteries, more variably placed in different patients. Thus, we prioritize the former branches so their hulls will be placed first and, therefore, experience less movement and deformation than the latter ones. An additional condition we impose is that no vessel hull be given higher priority than that of any of its ancestors. When the available region of the plane is not sufficient to place a hull, it needs to be deformed to fit into the region. A penalty function, discussed later, is computed to measure the deformation.

2) Radial Sweep Line Algorithm: Upon the setting of prioritization, an important subproblem is to determine the available region for a vessel hull to be placed. Suppose a hull ("target hull") is to be placed on the plane where several hulls have been placed beforehand. The origin of the target hull is fixed to a point on the arc of the parent hull. From this point we cast an imaginary ray in a given direction. If the ray hits a side of a hull, then that side restricts the possible placement of the target hull. We name such a side a "wall". (If the ray hits no hull then we consider the wall to lay infinitely far in that direction.) By casting rays in all directions we detect all the walls. This can be effectively done by a radial sweep line algorithm: There are only a finite number of points that contribute the event that the wall changes from one side to the other. Such event points can be found for each hull. Then the event points are sorted radially. By visiting those points in the sort order, one can determine which side is closest to the ray origin and therefore can decide the wall. The assumption of pre-placement of the parent hull rules out the hulls that lie on the same side of the half plane defined by the center of the target hull and the tangent of the arc of the parent hull at this point. This is because to avoid an overlap with the parent hull, the target hull must lie on the other side of the half plane.

3) Placement: The sweep line algorithm not only finds the available region for the placement but also subdivides the region into a set of triangular slices whose common vertex is the center of the target hull. The placement algorithm first fits circular sectors into a set of subregions made of all possible consecutive slices. For instance if the region consists of 3 slices, there are 3 subregions made of a single slice, 2 subregions made of two consecutive slices, and the entire available region made of three consecutive slices. Then the algorithm computes the penalty of deformation of the target hull for each circular sector. We use a penalty function which treats the effect of the area change and the rotation almost equally:

$$P = \left| \log \frac{A_{def}}{A_{org}} \right| + \left| \tan \frac{\phi}{4} \right|, \tag{1}$$

where A_{org} and A_{def} are the areas of the target hull before and after the deformation, and ϕ is the rotation angle between these two forms of the target hull. Notice that the penalty function (1) is zero when the target hull is placed without deformation.

The overall untangling is done by repeating the sweep line and the placement algorithm for each vessel hull in priority order. The deformation of vessel hulls transforms the vessel centerlines in a nonlinear manner, but cannot introduce any self-intersections.

D. Experiment

We tested our method using a database of real abdominal aortic trees, built from the collection of abdominal CT angiography from 10 patients (8 male, 2 female, ages 34-84) who were suspected to have vascular disease. Prior to transference to our workstation, all data were anonymized as required by HIPAA and our Institutional Review Board. Transverse CT images consisted of 512×512 pixels, reconstructed with fields of views (FOVs) ranging from 299 to 447 mm, with nominal section thickness varying from 0.625 to 1.25 mm. The number of slices per patient was between 508 and 693. Centerlines of the relevant vessels were extracted semi-automatically using a previously developed algorithm [4]. Each vessel centerline was stored as a sampled 3D curve. The anatomic label of each vessel was manually determined and associated with the corresponding centerline in order to form a binary tree data structure. Priority assignments, in order, were the abdominal aorta, the left and right common iliac arteries, the left and right renal arteries, the celiac artery, the superior mesenteric arteries, and the inferior mesenteric arteries. An anterior-posterior (A-P) viewing direction was

chosen for each patient to produce an orthographic projection. The resulting 2D views had false intersections mostly in the renal artery region and were used as an input to our untangling algorithm.

E. Evaluation

In order to quantify the effectiveness of the proposed visualization method, we defined several distortion metrics that summarize the key aspects of the method. As our untangling algorithm applies the stretched CPR to the curves and then scales and rotates the vessel hulls, the distortion metrics should incorporate those components. Notice that the resulting transformation from the orthographic projection to the untangled visualization is nonlinear and hard to formulate. We avoid such a difficulty by modeling the deformation as a pair of thin-plate splines (PTPS) [5]:

$$\Phi(t) = c + At + \sum_{j=1}^{k} w_j \, \sigma(t - t_j), \tag{2}$$

where $t \in \mathbb{R}^2$ is a point on the original curve (in the orthographic projection), k is the number of sample points, and

$$\sigma(h) \quad = \quad \begin{cases} \|h\|^2 \log(\|h\|), & \text{if } \|h\| > 0, \\ 0, & \text{if } \|h\| = 0. \end{cases}$$

The parameters c, A, and $w_j, \quad j = 1, \cdots, k$ are obtained subject to the constraints

$$y_j = \Phi(t_j) \ (j = 1, \cdots, k), \quad \sum_{j=1}^{k} w_j^T = 0, \quad \sum_{j=1}^{k} t_j w_j^T = 0,$$

where $y_j, j = 1, \cdots, k$ are the sample points on the deformed curve forming the untangled visualization. For more details on the PTPS, see [6].

The PTPS (2) models the deformation as a sum of an affine transform and a nonlinear transform called bending. The effect of scaling can thus be separately quantified as the affine scaling

$$\sqrt{d_{\max}(A) \, d_{\min}(A)} \tag{3}$$

which is a geometric mean of the singular values of the 2×2 affine matrix $A = UDV^T$ and the total bending energy

$$J(\Phi) = \text{trace}(W^T S W), \tag{4}$$

where $W = (w_1, \cdots, w_k)^T$ and $(S)_{ij} = \sigma(t_i - t_j)$.

Ideally the affine scaling (3) should be close to 1 and the bending energy (4) should be close to 0. Distortion metrics similar to (3) were used for texture mapping on meshes [7], [8]. Note that these metrics are both invariant under translation and rotation.

The degree of rotation is indirectly quantified by measuring the absolute difference of angles between pairs of vessels that share common branching points, *i.e.*, vessels that are in a parent-child relation or siblings. The resulting quantity is a symmetric matrix in which only entries corresponding to the aforementioned pairs of vessels are defined. We name this the pairwise angular distortion matrix.

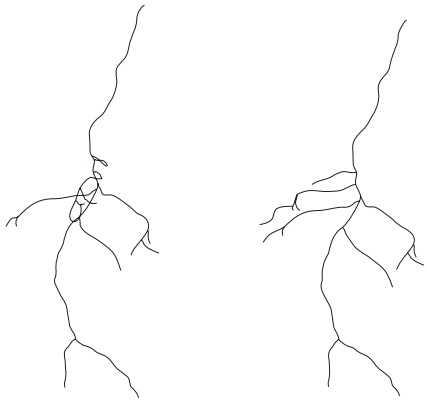

(a) (b)

Fig. 1. Anterior-posterior views of the abdominal aortic tree of an anonymous patient. (a) before untangling, (b) after untangling.

III. RESULTS

Table I gives the representative values of the introduced distortion metrics for all 10 cases in the test database. The mean and the maximum/minimum of each of the multiple-valued metrics are used as representatives. Geometric means are used for the affine scaling while arithmetic means are used for the other two. Note that for the pairwise angular distortion, the arithmetic mean is taken for the defined entries only. For the minima and the maxima the names of the vessels that attain those extreme values are also shown.

TABLE I

SUMMARY OF DISTORTION METRICS FOR THE ENTIRE DATA SET

	affine scaling			bending energy		pairwise angular	
patient	mean	max	min	mean	max	mean	max
1	1.048	1.742 (celiac)	0.8883 (IMA)	12.66	236.7 (celiac)	0.3279	1.435 (celiac)
2	0.8334	1.439 (celiac)	0.0890 (SMA)	0.08902	0.7575 (celiac)	0.2995	1.820 (celiac)
3	0.9004	1.406 (celiac)	0.1355 (SMA)	0.1131	1.038 (iliac)	0.2517	1.313 (SMA)
4(*)	0.9972	1.435 (celiac)	0.4303 (SMA)	63.63	1240 (celiac)	0.2147	1.091 (SMA)
5	0.9785	1.510 (celiac)	0.4865 (SMA)	0.6744	13.16 (celiac)	0.1505	0.4493 (SMA)
6	0.9056	1.308 (renal)	0.2093 (SMA)	1.482	15.85 (renal)	0.3546	2.997 (iliac)
7	1.034	1.588 (celiac)	0.8932 (SMA)	2.536	37.92 (SMA)	0.2859	2.009 (SMA)
8	0.7592	1.167 (renal)	0.0723 (SMA)	0.9662	17.61 (celiac)	0.4143	2.941 (SMA)
9	0.9444	1.232 (renal)	0.3183 (celiac)	2.126	25.70 (celiac)	0.6606	2.249 (renal)
10	0.8195	1.346 (celiac)	0.0622 (aorta)	0.5140	6.590 (SMA)	0.5251	2.570 (IMA)

Figure 1 shows the input orthographic projection and the output untangled visualization for the case marked with an asterisk in Table I. One can see that all the false intersections are completely resolved while the overall shape is well preserved. The full distortion metrics for this case are plotted in Fig. 2 for further discussion in Section IV.

Table I shows that the scale is maintained close to unity and that the spatial relaxation is performed mostly by rota-

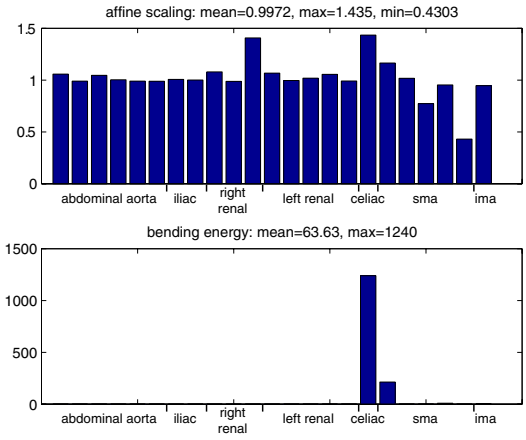

(a) Affine scaling and bending energy distortion

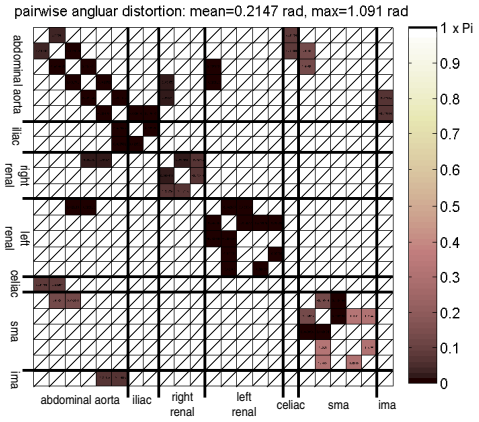

(b) Visualization of the pairwise angular distortion matrix. Bright shading represents high distortion. Undefined entries are not shaded and marked using oblique lines. The maximum distortion is about 0.35π.

Fig. 2. Distortion metrics for the visualization shown in Fig. 1.

tion. We postpone the discussion of the role of the bending energy to section IV. The extreme values listed in the cases of the celiac and the superior mesenteric arteries indicate that these arteries suffer the most severe distortion. This result agrees with our observation of the output visualizations. This is natural because in an anterior-posterior view, those ventral arteries are almost perpendicular to the display plane and their spatial configuration need to be modified to appear to lie in the plane of view.

IV. DISCUSSION

While the mean affine scaling and the mean pairwise angular distortion in Table I are relatively constant across the 10 patients, the mean bending energy varies considerably more. Moreover, although the quality of the untangled visualization shown in Fig. 1 is perceptually good, Table I indicates that this case had the largest bending energy among the data sets. To see why, we decompose the algorithm into two phases.

The first phase "stretches" the vessels in the orthographic projection. The untangling operation performed in the second phase involves the scaling and rotation of the vessel hulls. Although it transforms the stretched vessels nonlinearly, the degree of nonlinearity is relatively small compared to that of the stretched CPR performed in the first phase, especially when the deformation of the hulls is minimized as the algorithm aims. Therefore we expect that the most of the bending occurs in the first phase while the relatively large scaling or rotation occurs in the second phase. Although not shown here due to the space limitation, distortion metrics computed separately for these two phases confirms the conjecture. Comparing the celiac arteries in Figs. 1(a) and 1(b), one can see that the mapping between these two curves is highly nonlinear, thus large bending energy mostly comes from the first phase.

This observation shed light toward a possible further improvement to the method. A problem of the current algorithm is that vessels with a low priority may suffer a lack of available region and, as a result, undergo severe nonlinear deformation. Such a case can be easily detected by the extreme value of the bending energy, which may be fed back to the algorithm to resolve the situation, possibly by slightly permuting the priority order. This approach can also enhance the scalability of the algorithm.

V. CONCLUSIONS

We presented a 2D visualization algorithm for the abdominal aorta and its branches. The algorithm is capable of eliminating misleading false intersections in conventional projections, while conserving the overall shape of the vasculature. We also proposed several distortion metrics to quantify the relaxation of the spatial configuration of vessels, and evaluated these metrics on a database of 10 CT angiograms. These metrics agree well with the visual perception of the resulting map, and can signal extreme behavior of the algorithm. Future work will exploit the advantage of such quantification.

REFERENCES

[1] L. Saroul and O. Figueiredo, "Distance preserving flattening of surface sections," *IEEE Trans. Vis. Comp. Graphics*, vol. 12, no. 1, pp. 26–35, 2006.

[2] A. Kanitsar, R. Wegenkittl, D. Fleischmann, and M. E. Gröller, "Advanced Curved Planar Reformation: Flattening of Vascular Structures," in *IEEE Visualization 2003*, Oct. 2003, pp. 43–50.

[3] A. Kanitsar, D. Fleischmann, R. Wegenkittl, P. Felkel, and M. E. Gröller, "CPR - Curved Planar Reformation," in *IEEE Visualization 2002*, Oct. 2002, pp. 37–44.

[4] R. Raman, S. Napel, C. F. Beaulieu, E. S. Bain, R. B. Jeffrey, Jr, and G. D. Rubin, "Automated generation of curved planar reformations from volume data: Method and evaluation," *Radiology*, vol. 223, no. 1, pp. 275–80, 2002.

[5] F. L. Bookstein, "Principal warps: Thin-plate splines and the decomposition of deformations," *IEEE Trans. Pattern Anal. Mach. Intell.*, vol. 11, no. 6, pp. 567–585, 1989.

[6] I. L. Dryden and K. V. Mardia, *Statistical Shape Analysis*. John Wiley & Sons, 1998.

[7] P. V. Sander, J. Snyder, S. J. Gortler, and H. Hoppe, "Texture mapping progressive meshes," in *SIGGRAPH '01*, 2001, pp. 409–416.

[8] O. Sorkine, D. Cohen-Or, R. Goldenthal, and D. Lischinski, "Bounded-distortion piecewise mesh parameterization," in *IEEE Visualization 2002*, Oct. 2002, pp. 355–362.